ACS Macro Letters

pubs.acs.org/macroletters Letter

Cationic Bottlebrush Polymers Outperform Linear Polycation Analogues for pDNA Delivery and Gene Expression

Rishad J. Dalal, Ramya Kumar, Monica Ohnsorg, Mary Brown, and Theresa M. Reineke*

Cite This: ACS Macro Lett. 2021, 10, 886−893 Read Online

ACCESS | Metrics & More | Article Recommendations | Supporting Information

ABSTRACT: Cationic polymer vehicles have emerged as promising platforms for nucleic acid delivery because of their scalability, biocompatibility, and chemical versatility. Advancements in synthetic polymer chemistry allow us to precisely tune chemical functionality with various macromolecular architectures to increase the efficacy of nonviral-based gene delivery. Herein, we demonstrate the first cationic bottlebrush polymer-mediated pDNA delivery by comparing unimolecular, synthetically defined bottlebrush polymers to their linear building blocks. We successfully synthesized poly(2-(dimethylamino)ethyl methacrylate) (pDMAEMA) bottlebrushes through ring-opening metathesis polymerization to afford four bottlebrush polymers with systematic increases in backbone degree of polymerization (N_{bb} = 13, 20, 26, and 37), while keeping the side-chain degree of polymerization constant (N_{sc} = 57). Physical and chemical properties were characterized, and subsequently, the toxicity and delivery efficiency of pDNA into HEK293 cells were evaluated. The bottlebrush-pDNA complex (bottleplex) with the highest N_{bb}, BB_37, displayed up to a 60-fold increase in %EGFP+ cells in comparison to linear macromonomer. Additionally, we observed a trend of increasing EGFP expression with increasing polymer molecular weight. Bottleplexes and polyplexes both displayed high pDNA internalization as measured via payload enumeration per cell; however, quantitative confocal analysis revealed that bottlebrushes were able to shuttle pDNA into and around the nucleus more successfully than pDNA delivered via linear analogues. Overall, a canonical cationic monomer, such as DMAEMA, synthesized in the form of cationic bottlebrush polymers proved to be far more efficient in functional pDNA delivery and expression than linear pDMAEMA. This work underscores the importance of architectural modifications and the potential of bottlebrushes to serve as effective biomacromolecule delivery vehicles.

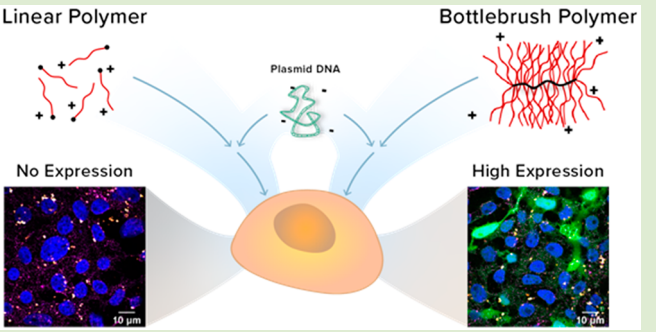

Polymeric vehicles are a versatile platform for the delivery of nucleic acids and offer numerous advantages over viral vectors by potentially enabling lower immunogenicity and production costs along with facile scalabilty.[1] Cationic polymers readily complex negatively charged nucleic acids through an entropically driven displacement of counterions to form interpolyelectrolyte complexes. Beyond linear cationic homopolymers, the field is being transformed through exploration of the vast chemical and architectural space afforded by recent advances in synthetic control to develop statistical and block linear copolymers, self-assembled micelles, stars, dendrimers, and cross-linked networks in an effort to overcome limitations in transfection efficiency.[1−4] Our earlier work, harnessing reversible addition−fragmentation chain transfer (RAFT) polymerization techniques to synthesize triblock micelles, has demonstrated how control over polymer architecture can lead to high delivery efficiency without increasing toxicity, despite increasing the density of cations within the self-assembled micelle corona.[5−8] That work compared spherical micelles to linear polymer analogues and highlighted how micelle complexes (micelleplexes) outperform polyplexes in delivery efficacy due to structural maintenance of the biological payload. This demonstrated the formation of polycationic micelles that induce high amine density within the corona is key for improving transfection efficiency. However, the self-assembly required to form micelles followed by a secondary formulation step can lead to challenges in scale-up.[9,10] Indeed, the ability to create well-defined unimolecular architectures, consisting of covalently linked cationic polymer chains clustered within a fixed volume, could facilitate a similar performance to cationic self-assembled micelles while granting more complete synthetic control and reproducibility over the macromolecular architecture.

Bottlebrush (BB) polymers are well-defined unimolecular architectures made up polymer side-chains that are covalently attached to and extend radially from a central polymer

Received: May 14, 2021
Accepted: June 17, 2021

https://doi.org/10.1021/acsmacrolett.1c00335
ACS Macro Lett. 2021, 10, 886−893

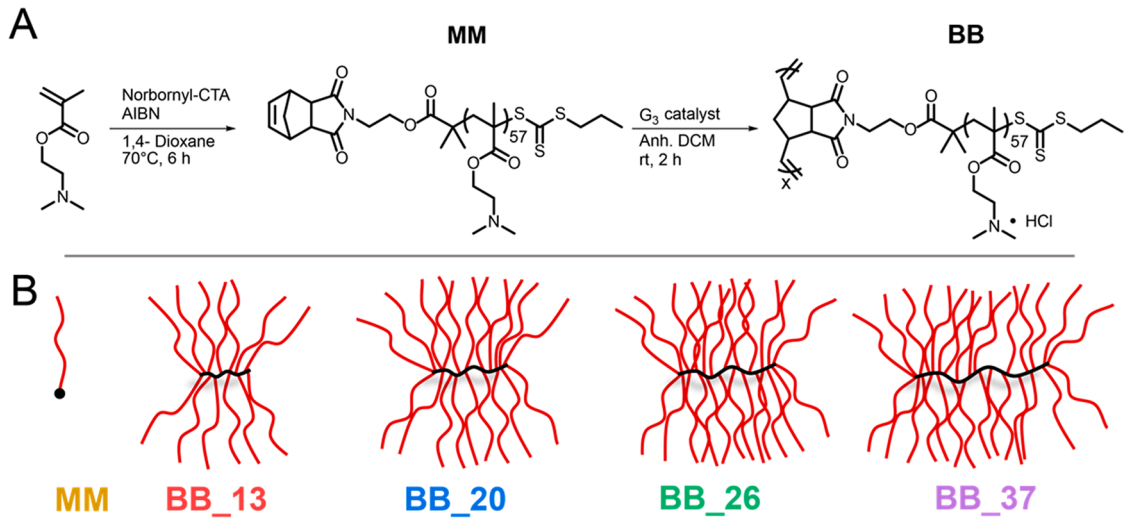

Figure 1. (A) Chemical scheme showing a two-step orthogonal polymerizations of RAFT polymerization followed by ROMP to achieve bottlebrush polymers with pendant tertiary amines. (B) Illustration of the bottlebrush (BB) polymer library synthesized from one macromonomer (MM). Bottlebrush names are defined by the number of repeat units in the backbone.

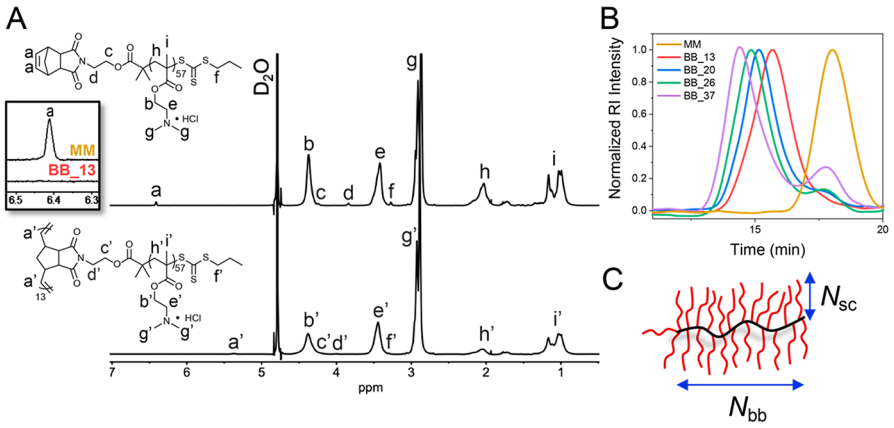

Polymer	M_n (kDa)	M_w (kDa)	$Đ$	N_{sc}:N_{bb}	% BB
MM	9.4	11	1.17	57:1	N/A
BB_13	124	143	1.15	57:13	>95
BB_20	184	220	1.20	57:20	90
BB_26	246	309	1.25	57:26	90
BB_37	344	458	1.33	57:37	81

Figure 2. (A) Stacked ^{1}H NMR spectra showing the conversion of peak a to a′ in MM (top) and BB_13 (bottom) spectra. (B) Stacked normalized differential refractive index (RI) showing conversion of MM to the four bottlebrushes. (C) Illustration showing nomenclature of degree of polymerization of side-chain (N_{sc}) and the backbone (N_{bb}). (D) Summary of SEC-MALS analysis of molecular weight distributions.

backbone. The polymers are created through polymerization of macromonomers (MM). The physical properties of such systems depend on the molar mass, degree of polymerization, and composition of both the side-chains and backbone.[11,12] The unique ability to synthetically alter and isolate these variables by using orthogonal polymerization techniques such as RAFT polymerization[13−15] and ring-opening metathesis polymerization (ROMP)[16−18] can be harnessed by different synthetic methods, including grafting-through and grafting-from techniques.[19−21] This synthetic platform also allows for the production of high molecular weight polymers while having relative control over dispersity. Bottlebrush polymers have shown efficacy for delivery of small molecule therapeutics by both covalent binding and noncovalent sequestration of the payload.[22−24] Only a few examples of using bottlebrush polymers for nucleic acid delivery have been documented to date. Schmidt et al. reported successful siRNA complexation, delivery, and gene silencing using bottlebrushes containing poly-L-lysine-*b*-polysarcosine polymer side-chains.[25] Zhang et al. covalently conjugated oligonucleotides and siRNA to poly(ethylene glycol) (PEG) bottlebrush systems and demonstrated resistance to nonspecific protein adhesion as

https://doi.org/10.1021/acsmacrolett.1c00335
ACS Macro Lett. 2021, 10, 886−893

well as increased *in vivo* biodistribution.[26−28] The effect of a cylindrical systems compared to spherical systems without biological payloads was observed to increase circulation time of cylindrical systems correlated to its increased aspect ratio.[29,30]

Despite the numerous advantages of bottlebrush systems, their capacity to deliver larger biological payloads like plasmids (pDNA) has not yet been investigated. Unlike siRNA and oligonucleotides, pDNA payloads present unique challenges as the long semiflexible structure imposes additional constraints on their polymeric binding partners during polymer−pDNA assembly and compaction. Moreover, unlike other nucleic acid payloads, they can only accomplish their therapeutic function when delivered to the nucleus. In this work, we have exploited the unique architectural and morphological features of bottlebrush systems and overcome delivery challenges specific to pDNA payloads. Bottlebrushes offer three main advantages for delivery of pDNA over previously published architectural systems: (1) bottlebrushes have proven to be synthetically reproducible while offering a high molecular weight unimolecular synthetic platform to tailor isolated variables of grafting density, side-chain length, backbone length, and chemistry; (2) densely grafted bottlebrush systems offer physical changes to multivalency, charge, and binding; and (3) unlike other polymeric gene delivery systems to date, bottlebrush polymers offer high-aspect-ratio systems with the potential to improve *in vivo* delivery outcomes and facilitate control over biodistribution profiles.

Herein, we present the first exploration of cationic bottlebrush polymers for noncovalent binding and delivery of pDNA payloads. We synthesized a library of cationic bottlebrush polymers with systematic increases in backbone degree of polymerization (N_{bb}), while keeping the side-chain degree of polymerization (N_{sc}) constant (Figures 1 and 2B). When assessing the discrete role of architecture and size on the chemical and physical properties of these polymer vectors, it was found that the bottlebrushes and linear macromonomer had similar pK_a values, formed polymer−pDNA complexes of comparable sizes, and resulted in similar cellular toxicities. Interestingly, these bottlebrush polymers showed lower comparative binding strength, lower protonation degree at physiological pH, and higher nuclear colocalization of pDNA with the bottlebrush as compared to the macromonomer. This work is the first to show that bottlebrush polymers significantly increase the delivery of pDNA when compared to linear polymer analogues when holding the chemistry and formulation ratios for amine concentration consistent. Herein reveals that efficacy is a function of bottlebrush molecular weight, with increased N_{bb} resulting in improved delivery performance. Overall, this work demonstrates the ability of these powerful macromolecules to broadly serve as readily tailorable supramolecular hosts for delivery of large biomolecular payloads.

To synthesize the target family of bottlebrush polycations, we first performed RAFT polymerization of an amine-based monomer, 2-(dimethylamino)ethyl methacrylate (DMAEMA), with a norbornene-functionalized chain transfer agent (CTA), to yield linear macromonomers with a number-average molecular weight (M_n) of 9.4 kDa. The degree of polymerization was found to be higher than theoretical, likely due to the trithiocarbonate R-group being optimized for polymerization of acrylates/acrylamides rather than methacrylates/methacrylamides. The bottlebrush polymers were synthesized through ROMP of the norbornene imide end-group on the macromonomer by varying the mole ratio of Ru-based third-generation Grubbs catalyst to achieve bottlebrush polymers with systematic increases in molecular weight equating to N_{bb} repeat units of 13, 20, 26 and 37, while maintaining a relatively low dispersity ($Đ \leq 1.33$, Figure 2D). Size exclusion chromatography with a multiangle laser light scattering detector was used to characterize molecular weight and dispersity (Figure 2B,D), and ^{1}H NMR was used to identify conversion of the norbornene alkene (Figure 2A and Figure S2).

The protonation state of the multivalent bottlebrushes was characterized via acid−base titrations. Particularly, we sought to understand if the collective density of linear polymers assembled in the fixed volume of the bottlebrush architecture would lead to pK_a changes in the physiological pH range, which could alter binding interactions between the polycationic polymers and the polyanionic pDNA payload. The pK_a decreased by 1.4 units from monomer (DMAEMA, pK_a = 8.5) to linear polymer (macromonomer, pK_a = 7.1), as supported by previous literature findings showing the suppression of amine ionization and proximity to charged groups upon polymerization.[31,32] However, when comparing the bottlebrush polymers to the macromonomer, similar pK_a values were found (Figure 3A). Uniquely, at physiological pH

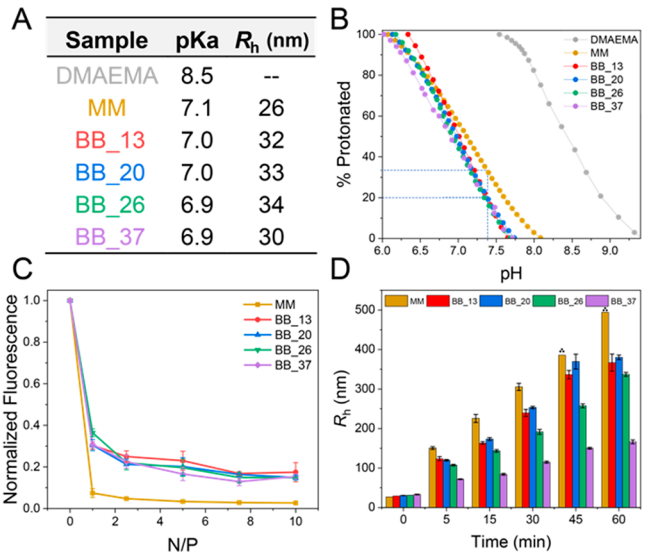

Figure 3. (A) pK_a data of monomer and polymers acquired from acid−base titration and R_h data of polyplexes and bottleplexes formed in H_2O acquired from DLS. (B) Standardized protonation states of monomer and polymers calculated from titration data. Dotted blue line shows percent of polymer protonated at pH 7.4 (C) Fluorescence analyzed through dye exclusion of PicoGreen. (D) R_h data acquired from DLS of polyplexes and bottleplexes formed in water (t = 0 min) and then aggregation of the complexes over 60 min after addition of Opti-MEM. Error bars are represented by ± standard deviation of analyzed data (n = 3). The "∴" indicates the inability to acquire replicate measurements due to severe aggregation and poor autocorrelation functions.

of 7.4, bottlebrush polymers are ∼10% less protonated than the macromonomer, indicating a dissimilarity of the charged state of the polymers (see dotted lines in Figure 3B). This property could influence charge-mediated interactions and compaction/decompaction of pDNA payloads at physiological conditions.

https://doi.org/10.1021/acsmacrolett.1c00335
ACS Macro Lett. 2021, 10, 886−893

Polymer-pDNA/bottlebrush-pDNA complexes, termed polyplexes/bottleplexes, were analyzed for compaction ability and binding strength through gel electrophoresistential, ζ-potential, and dye exclusion. Assays were completed by varying the number ratio of amines (N) in the polymer to phosphates (P) in the nucleic acid backbone (N/P ratio) to determine a minimum binding capacity. It is worth noting that with this formulation ratio the number/concentration of amines in solution are equal at each formulation ratio for each material. However, going from macromonomer to bottlebrushes of increasing molecular weight, the number of discrete polymer chains in solution decreases (as macromonomers successively covalently stitched together). Qualitative image analysis of the gel electrophoresis shift assay showed complete hindrance of pDNA migration at N/P of 1.5 and higher (Figure S7) for all formulations. This work thus establishes the successful complexation and compaction of pDNA using bottlebrush polymers at low formulation ratios for all polymer architectures. When the five polymer formulations at N/P of 7.5 were measured for ζ-potential, all polymer complexes show positive charge ranging from 27 to 35 mV for the bottleplexes, while the macromonomer had an increased charge at 43 mV (Figure S9).

A dye exclusion assay helped gain further insight into the degree of pDNA compaction when complexed with these polycations, which involves the release of a fluorescent intercalating dye when competitive agents (the cationic macromonomer or bottlebrushes) are introduced, and no longer fluoresces when excluded from the pDNA. The macromonomer showed more displacement of the dye from pDNA in comparison to the bottlebrushes, with all four bottlebrush polymers displaying an averaged 5-fold higher fluorescence at each N/P ratio (Figure 3C). Subsequently, the gel electrophoresis shift assay showed no free pDNA above N/P 1.5, and therefore it is hypothesized that the difference in fluorescence intensity between the macromonomer and the bottlebrushes can be attributed to be the degree of pDNA compaction. The bottlebrush polymers exist as a multivalent display of linear polycations that, conformationally, are more outstretched than the macromonomers, which likely exist as random coils in solution. The difference in solution structure of the bottlebrush systems could alter the binding mode, where the pDNA associates more superficially with the bottlebrush surface while the more flexible linear MMs could bind more intimately in the major or minor grooves, thereby displacing the intercalating dyes.

To further test the stability of these systems against competitive binding factors such as serum proteins, the polyplex/bottleplex solutions were diluted 2-fold with a 10% fetal bovine serum (FBS) solution. There was an increase in dye fluorescence after introduction of FBS, and the macromonomer had an averaged 40% increase in fluorescence, while the bottlebrushes averaged a 20% increase. These results interestingly showed slightly better serum stability for bottlebrushes compared to the linear analogue (Figure S8). Although the linear macromonomer and bottlebrush polymers have similarity in chemical functionality and pK_a, the macromolecular structure of the bottlebrush polymers appears to significantly influence the mode of pDNA binding and compaction, which may, in turn, influence intracellular release.

The size and aggregation behavior of these interpolyelectrolyte complexes have shown to have some effect on delivery efficacy of nucleic acids into cells.[30] Hydrodynamic radii (R_h) of polyplexes and bottleplexes were analyzed via dynamic light scattering after formation. The polyplexes and bottleplexes all formed similar sized complexes in water ($R_h \sim 30$ nm, Figure S6) and did not aggregate over time, showing that macromolecular architecture did not alter the polyionic complex size during initial formulation. To understand size and stability during the transfection conditions, the formulations were further diluted in Opti-MEM and monitored for stability. Throughout the 60 min period, aggregation was observed among all five interpolyelectrolyte systems. However, the macromonomer polyplexes aggregated to the largest size. A trend was observed where increasing the bottlebrush molecular weight correlated to a decrease in the aggregation behavior. After 60 min, the bottlebrush with the longest backbone, BB_37, displayed the lowest size in Opti-MEM (R_h = 165 nm) and had a 3-fold decrease in size compared to the macromonomer (R_h = 495 nm, Figure 3D). The ability to tailor bottleplex size distribution and control aggregation via synthetic control with ROMP makes this delivery platform attractive for future *in vivo* applications.

The primary goal of constructing this polymer library was to create hierarchical unimolecular structures with increasing N_{bb} and directly compare the transfection ability of the bottlebrush series to the linear macromonomer building block. We employed an enhanced green fluorescent protein (EGFP) reporter assay to gain insight into the polymer vehicle's ability to deliver pDNA into cells and express the encoded protein. To test this, a solution containing the plasmid construct encoding for EGFP were mixed in formulation ratios at N/P ratios of 5, 7.5, and 10 with the macromonomer or one of four bottlebrushes and allowed to complex for 45 min in water before being further diluted in Opti-MEM and layered onto human embryonic kidney (HEK293) cells. Transfection and flow cytometry procedures are detailed in the Supporting Information. The differences observed in %EGFP positive cells observed by flow cytometry and fluorescence microscopy revealed a vast difference in transfection efficiency between the macromonomer and the bottlebrush formulations (Figure 4A and Figure S15). Surprisingly, macromonomer was unable to produce any notable amount of %EGFP positive cells (<1.5%), while the bottlebrush polymers ranged from 28 to 60% EGFP positive cells, depending on N/P ratio and N_{bb}. Previous studies in our group tested a 25 kg/mol pDMAEMA polymer[6] which also delivered pDNA to HEK293 cells and resulted in ~5% GFP expression. This 25 kg/mol pDMAEMA is 2.5 times longer than our MM and yet did not result in a commensurate improvement in transfection performance over our macromonomer. This previous work indicates that the sole factor of increasing molecular weight of a linear pDMAEMA control will not have a significant impact on pDNA delivery performance. An average 1.5-fold increase in %EGFP positive cells was observed between N/P ratio of 5 and 10. At each N/P ratio, BB_37 had an average 1.5-fold increase of %EGFP positive cells compared to BB_13, suggesting that N_{bb} (and thus molecular weight) is positively correlated to transfection efficiency. Positive controls of Lipofectamine 2000 and jetPEI displayed high transfection performance as expected, with 97% and 89% EGFP positive cells, respectively (Figure S10). ANOVA statistical analysis confirmed statistical significance in the performance difference between macromonomer and BB_13 as well as BB_13 from BB_37 at all three N/P ratios. Both BB_13 and BB_37 also are statistically different from themselves at polymer ratios of N/P 5 from 10, showing an

https://doi.org/10.1021/acsmacrolett.1c00335
ACS Macro Lett. 2021, 10, 886−893

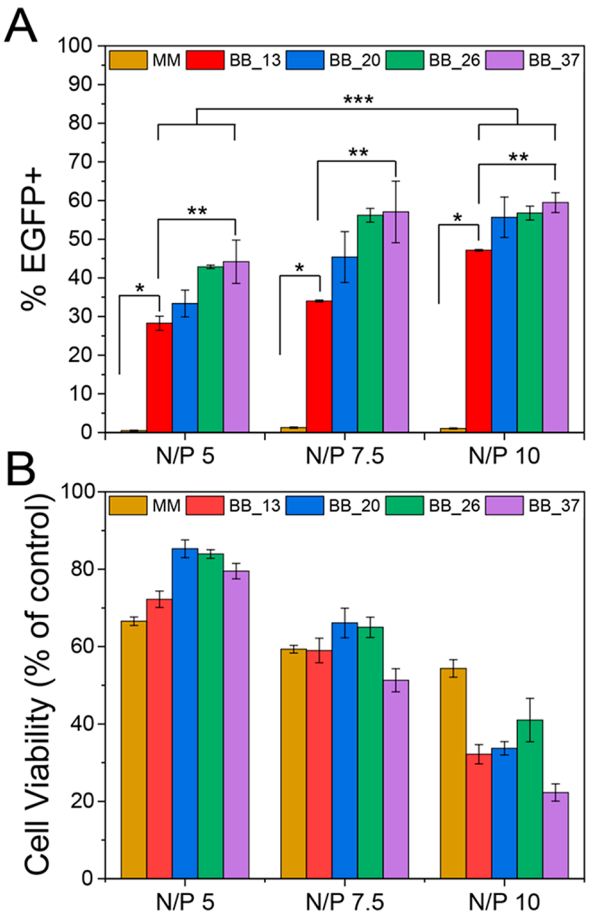

Figure 4. (A) Flow cytometry data showing percent EGFP positive HEK293 cells due to delivery with MM and BBs at N/P ratios of 5, 7.5, and 10. The asterisks (∗) indicate statistical difference ($p < 0.05$) analyzed by one-way ANOVA followed by a *post hoc* Tukey test. (B) Cell viability data as measured via CCK-8 assay with HEK293 cells with complexes formed at N/P ratios of 5, 7.5, and 10. Error bars are represented by ± standard deviation of analyzed data ($n = 3$).

increase in transfection efficiency with an increase in formulation ratio. This data displays how chemical architecture can play a significant role in improving delivery efficiency by having up to a 60-fold increase of EGFP positive cells when comparing BB_37 to the macromonomer.

Cell viability was measured with cell counting kit-8 (CCK-8) to understand the active metabolic process in the cell populations after transfection. Cells underwent the same transfection procedures with each formulation and were then subjected to UV-absorbance analysis of the CCK-8 dye 48 h after initial transfection (procedures are in the Supporting Information). As seen in Figure 4B, the cell viability was found to be similarly high for all formulations at the N/P ratios of 5 and 7.5 and found to have higher cell viability than both commercial controls of Lipofectamine 2000 and jetPEI (Figure S12). A higher toxicity profile was found at N/P = 10, with the macromonomer displaying similar levels of viable cells to jetPEI and the four bottlebrush polymers exhibiting cell viability similar to Lipofectamine 2000. This shows that the increased size and charge density of the higher ordered bottlebrush architectures were not accompanied by significantly higher levels of cellular toxicity when compared to the smaller macromonomer.

To probe whether the stark difference in transfection efficiency can be attributed to differences in cellular uptake between polyplexes/bottleplexes, we measured internalization by using fluorescently labeled cyanine 5 (Cy5)-pDNA. Cells administered with all five delivery vehicle formulations showed similarly high Cy5 fluorescence intensities (>90% positive) showing little discrepancy in Cy5 intensities between the macromonomer and bottlebrush complexes (Figure S13). This data suggests that transfection is not limited by cellular internalization; rather, bottleplexes appear to overcome some intracellular hurdle for successful expression.

To examine the intracellular localization of polyplexes/bottleplexes, HEK293 cells were transfected with macromonomer and BB_37 complexes formulated at N/P of 7.5, and the cells were fixed 24 h following pDNA delivery. To facilitate pDNA visualization, fluorescent polyplexes were formulated by using Cy5-pDNA payloads; the outlines of lysosomal compartments were labeled by LAMP-2 and the nuclei stained with Hoechst. Consistent with observations from flow cytometry, both complexes were internalized efficiently, as indicated by the appearance of multiple Cy5 signals associated with the pDNA enumerated within cells (Figure 5). Visually, the

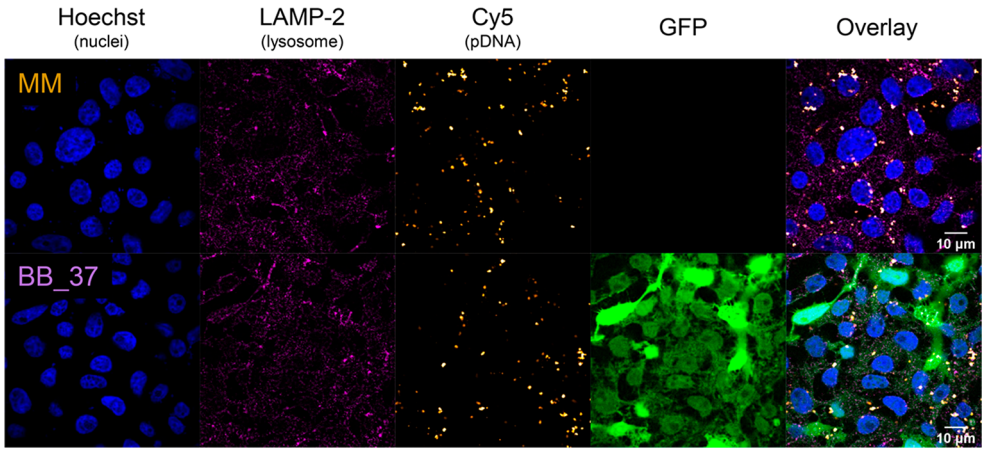

Figure 5. Confocal 2D images comparing MM and BB_37 by tracking Cy5-labeled pDNA internalized into HEK293 cells, cells fixed at 24 h. Confocal microscopy observations: nuclear Hoechst stain (blue), lysosomal LAMP-2 stain (magenta), Cy5-pDNA fluorescent tag (yellow), and EGFP produced (green). Scale bar 10 μm.

https://doi.org/10.1021/acsmacrolett.1c00335
ACS Macro Lett. 2021, 10, 886−893

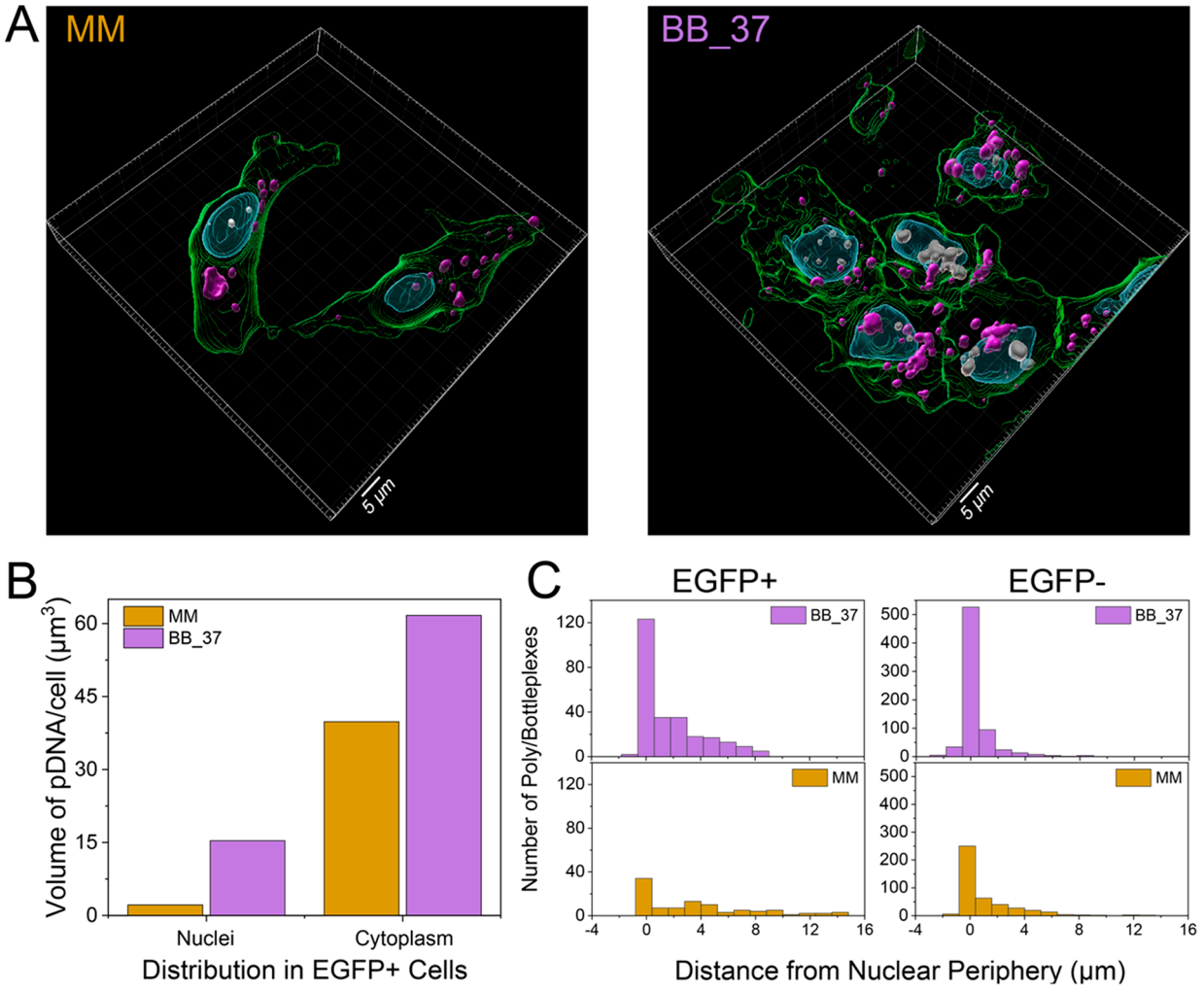

Figure 6. (A) Confocal 3D images comparing MM and BB_37 by tracking Cy5 labeled pDNA internalized into EGFP positive cells. Confocal microscopy observations: nuclear (blue), EGFP in cell cytoplasm (green), Cy5-pDNA in nucleus (white), and Cy5-pDNA in cytoplasm (magenta). Scale bar 5 μm. (B) Normalized volume (μm^3) of pDNA per EGFP positive cell in the nucleus and cytoplasm when transfected with MM and BB_37 determined by quantitative image analysis 24 h after initial transfection. (C) Distribution of polyplexes/bottleplexes from the periphery of the nucleus in EGFP+ and EGFP− cells analyzed from confocal analysis. Negative distance lengths indicate the centroid of the pDNA complex is within the nucleus.

macromonomer and BB-37 appear similarly colocalized when stained for LAMP-2 to label lysosomes and Cy5-pDNA (Figure S16 and S17), and this was confirmed quantitatively with Pearson's correlation coefficients. We note that the macromonomer displays higher colocalization (Table S2) with LAMP-2 than BB_37 in EGFP-positive and negative cells and that both macromonomer and BB_37 exhibit moderate colocalization within and outside EGFP-positive cells. Despite high cellular densities of polyplexes, payloads delivered by using the macromonomer did not culminate in EGFP expression, while in contrast very high intensities of EGFP were observed when treated with BB_37 bottleplexes, which was consistent with the flow cytometry data.

To assess the origins of gene expression disparity in functional payload delivery between the linear macromonomer polyplexes and the BB_37 bottleplexes, four to five Z-stacked confocal scans were acquired in the cell images per treatment group. From 3D reconstructions of EGFP-positive cells within each group, nuclear colocalized pDNA (white) and cytoplasmic colocalized pDNA (magenta) were able to be distinguished (Figure 6A). To quantitatively understand differences in nuclear translocation between bottleplexes and polyplexes, the volume occupied by Cy5-labeled pDNA was calculated, and distances between Cy5-labeled pDNA to the nuclear periphery were mapped. Both sets of analyses were performed separately for EGFP-positive as well as EGFP-negative cellular populations. Among the EGFP-positive cells, we observed over 1.5 times more total volume of Cy5-pDNA per cell in the cytoplasm and over 7-fold increase in total volume of Cy5-pDNA per cell in the nucleus when delivered by BB_37 compared to macromonomer (Figure 6B and Table S1). When considering the distribution of the pDNA from the periphery of the nucleus among EGFP-positive and EGFP-negative cells, more pDNA was internalized and was shuttled closer to the nuclei by BB_37 (Figure 6C). Commercial controls such as Lipofectamine[33] and JetPEI[34] have been previously studied to show how an increased delivery of pDNA to and around the nucleus was correlated to higher gene expression. These studies further support the confocal findings that BB_37 delivered higher amounts of functional pDNA closer and to the nucleus, thus resulting in high transfection efficacy. Overall, quantitative confocal microscopy revealed

https://doi.org/10.1021/acsmacrolett.1c00335
ACS Macro Lett. 2021, 10, 886−893

that the distribution of pDNA payload accumulation within nuclear and cytoplasmic regions varied significantly, depending on whether they were shuttled into cells by polyplexes or bottleplexes. It is clear that bottleplexes deliver more pDNA into cells and shuttle pDNA closer to the nucleus. This increase in total pDNA uptake via nuclear trafficking effected by BB_37 bottleplexes likely contributed to the higher levels functional EGFP expression compared to the macromonomer polyplexes.

In conclusion, our work represents the first example of the synthesis, characterization, and application of a polycationic bottlebrush platform toward the delivery of pDNA payloads. We successfully applied ROMP to create a series of four bottlebrush polymers with increasing N_{bb} while keeping N_{sc} fixed from one batch of linear pDMAEMA macromonomer. Although the bottlebrush polymers and the macromonomer had similar chemical functionality, pK_a values, polyplex/bottleplex R_h sizes, toxicities, and internalization efficiencies, bottleplex BB_37 produced a 60-fold increase in EGFP-positive cells compared to the macromonomer building block. Flow cytometry further showed that while all bottlebrush formulations had similar internalization, increasing N_{bb} displayed on average a 1.5-fold increase in percentage EGFP-positive cells, when comparing BB_13 to BB_37. Interestingly, quantitative confocal microscopy affirmed that bottlebrush polymers deliver more pDNA into cells and also traffic pDNA closer to the nucleus than the macromonomer resulting in the highest transgene expression with BB_37. Although the polymer libraries were all constructed from the same cationic repeat unit, pDNA complexes were formed in the same amine concentrations, and similar levels of cellular uptake were found across the formulations, the unimolecular architectures of the bottlebrushes overcame key intracellular hurdles to achieve functional pDNA delivery to the nucleus. Ongoing efforts are aimed at understanding the biological mechanisms of delivery of these bottlebrush polymers as well as modifying the bottlebrush architecture to optimize transfection efficacy, colloidal stability, and further mitigation of toxicity.

■ ASSOCIATED CONTENT

Supporting Information

The Supporting Information is available free of charge at https://pubs.acs.org/doi/10.1021/acsmacrolett.1c00335.

^{1}H NMR spectra of representative polymers, SEC-MALS, $\partial n/\partial c$, pK_a titrations, gel electrophoresis, dye exclusion, EGFP transfection, cell viability, Cy5 internalization, confocal analysis, and experimental assay procedures and data (PDF)

Movie S1 (MP4)

Movie S2 (MP4)

■ AUTHOR INFORMATION

Corresponding Author

Theresa M. Reineke − *Department of Chemistry, University of Minnesota, Minneapolis, Minnesota 55455, United States;* orcid.org/0000-0001-7020-3450; Email: treineke@umn.edu

Authors

Rishad J. Dalal − *Department of Chemistry, University of Minnesota, Minneapolis, Minnesota 55455, United States*

Ramya Kumar − *Department of Chemistry, University of Minnesota, Minneapolis, Minnesota 55455, United States;* orcid.org/0000-0002-8725-0023

Monica Ohnsorg − *Department of Chemistry, University of Minnesota, Minneapolis, Minnesota 55455, United States;* orcid.org/0000-0002-7616-3880

Mary Brown − *University Imaging Centers, University of Minnesota, Minneapolis, Minnesota 55455, United States*

Complete contact information is available at: https://pubs.acs.org/10.1021/acsmacrolett.1c00335

Notes

The authors declare no competing financial interest.

■ ACKNOWLEDGMENTS

We thank DARPA (Contract N660011824041) for financial support of this project and the UIC Imaging Center and Guillermo Marques for their aid in confocal analysis. We also gratefully acknowledge Craig Van Bruggen and Cristiam F. Santa Chalarca for helpful discussions and Julia Holmes for help on the TOC design.

■ REFERENCES

(1) Kumar, R.; Santa Chalarca, C. F.; Bockman, M. R.; Van Bruggen, C.; Grimme, C. J.; Dalal, R. J.; Hanson, M. G.; Hexum, J. K.; Reineke, T. M. Polymeric Delivery of Therapeutic Nucleic Acids. *Chem. Rev.* **2021**, DOI: 10.1021/acs.chemrev.0c00997.

(2) Rinkenauer, A. C.; Schubert, S.; Traeger, A.; Schubert, U. S. The Influence of Polymer Architecture on in Vitro PDNA Transfection. *J. Mater. Chem. B* **2015**, *3* (38), 7477−7493.

(3) Qiu, L. Y.; Bae, Y. H. Polymer Architecture and Drug Delivery. *Pharm. Res.* **2006**, *23* (1), 1−30.

(4) Van Bruggen, C.; Hexum, J. K.; Tan, Z.; Dalal, R. J.; Reineke, T. M. Nonviral Gene Delivery with Cationic Glycopolymers. *Acc. Chem. Res.* **2019**. DOI: 10.1021/acs.accounts.8b00665.

(5) Sharma, R.; Lee, J.; Bettencourt, R. C.; Xiao, C.; Konieczny, S. F.; Won, Y. Effects of the Incorporation of a Hydrophobic Middle Block into a PEG-Polycation Diblock Copolymer on the Physicochemical and Cell Interaction Properties of the Polymer-DNA Complexes. *Biomacromolecules* **2008**, *9* (11), 3294−3307.

(6) Tan, Z.; Jiang, Y.; Zhang, W.; Karls, L.; Lodge, T. P.; Reineke, T. M. Polycation Architecture and Assembly Direct Successful Gene Delivery: Micelleplexes Outperform Polyplexes via Optimal DNA Packaging. *J. Am. Chem. Soc.* **2019**, *141* (40), 15804−15817.

(7) Tan, Z.; Jiang, Y.; Ganewatta, M. S.; Kumar, R.; Keith, A.; Twaroski, K.; Pengo, T.; Tolar, J.; Lodge, T. P.; Reineke, T. M. Block Polymer Micelles Enable CRISPR/Cas9 Ribonucleoprotein Delivery: Physicochemical Properties Affect Packaging Mechanisms and Gene Editing Efficiency. *Macromolecules* **2019**, *52* (21), 8197−8206.

(8) Jiang, Y.; Lodge, T. P.; Reineke, T. M. Packaging PDNA by Polymeric ABC Micelles Simultaneously Achieves Colloidal Stability and Structural Control. *J. Am. Chem. Soc.* **2018**, *140* (35), 11101−11111.

(9) Hayward, R. C.; Pochan, D. J. Tailored Assemblies of Block Copolymers in Solution: It Is All about the Process. *Macromolecules* **2010**, *43* (8), 3577−3584.

(10) Meli, L.; Lodge, T. P. Equilibrium vs Metastability: High-Temperature Annealing of Spherical Block Copolymer Micelles in an Ionic Liquid. *Macromolecules* **2009**, *42* (3), 580−583.

(11) Sheiko, S. S.; Sumerlin, B. S.; Matyjaszewski, K. Cylindrical Molecular Brushes: Synthesis, Characterization, and Properties. *Prog. Polym. Sci.* **2008**, *33* (7), 759−785.

(12) Müllner, M.; Müller, A. H. E. Cylindrical Polymer Brushes - Anisotropic Building Blocks, Unimolecular Templates and Particulate Nanocarriers. *Polymer* **2016**, *98*, 389−401.

(13) Chiefari, J.; Chong, Y. K.; Ercole, F.; Krstina, J.; Jeffery, J.; Le, T. P. T.; Mayadunne, R. T. A.; Meijs, G. F.; Moad, C. L.; Moad, G.; Rizzardo, E.; Thang, S. H. Living Free-Radical Polymerization by Reversible Addition - Fragmentation Chain Transfer: The RAFT Process We Wish to Report a New Living Free-Radical Polymer-Ization of Exceptional Effectiveness and Versatility. 1 The Living Character Is Conferred By. *Macromolecules* **1998**, *31*, 5559−5562.
(14) Perrier, S. 50th Anniversary Perspective: RAFT Polymerization - A User Guide. *Macromolecules* **2017**, *50* (19), 7433−7447.
(15) Moad, G. RAFT Polymerization- Then and Now. In *Controlled Radical Polymerization: Mechanisms*; Matyjaszewski, K., Ed.; American Chemical Society: Washington DC, 2015; pp 211−246.
(16) Runge, M. B.; Bowden, N. B. Synthesis of High Molecular Weight Comb Block Copolymers and Their Assembly into Ordered Morphologies in the Solid State. *J. Am. Chem. Soc.* **2007**, *129* (34), 10551−10560.
(17) Xia, Y.; Kornfield, J. A.; Grubbs, R. H. Efficient Synthesis of Narrowly Dispersed Brush Polymers via Living Ring-Opening Metathesis Polymerization of Macromonomers. *Macromolecules* **2009**, *42* (11), 3761−3766.
(18) Li, Z.; Zhang, K.; Ma, J.; Cheng, C.; Wooley, K. L. Facile Syntheses of Cylindrical Molecular Brushes by a Sequential RAFT and ROMP "Grafting-through" Methodology. *J. Polym. Sci., Part A: Polym. Chem.* **2009**, *47* (20), 5557−5563.
(19) Senkum, H.; Gramlich, W. M. Cationic Bottlebrush Polymers from Quaternary Ammonium Macromonomers by Grafting-Through Ring-Opening Metathesis Polymerization. *Macromol. Chem. Phys.* **2020**, *221* (5), 1900476.
(20) Radzinski, S. C.; Foster, J. C.; Chapleski, R. C.; Troya, D.; Matson, J. B. Bottlebrush Polymer Synthesis by Ring-Opening Metathesis Polymerization: The Significance of the Anchor Group. *J. Am. Chem. Soc.* **2016**, *138* (22), 6998−7004.
(21) Radzinski, S. C.; Foster, J. C.; Matson, J. B. Synthesis of Bottlebrush Polymers via Transfer-to and Grafting-through Approaches Using a RAFT Chain Transfer Agent with a ROMP-Active Z-Group. *Polym. Chem.* **2015**, *6* (31), 5643−5652.
(22) Johnson, J. A.; Lu, Y. Y.; Burts, A. O.; Xia, Y.; Durrell, A. C.; Tirrell, D. A.; Grubbs, R. H. Drug-Loaded, Bivalent-Bottle-Brush Polymers by Graft-through ROMP. *Macromolecules* **2010**, *43* (24), 10326−10335.
(23) Takano, S.; Islam, W.; Nakazawa, K.; Maeda, H.; Sakurai, K.; Fujii, S. Phosphorylcholine-Grafted Molecular Bottlebrush-Doxorubicin Conjugates: High Structural Stability, Long Circulation in Blood, and Efficient Anticancer Activity. *Biomacromolecules* **2021**, *22* (3), 1186−1196.
(24) Ohnsorg, M. L.; Prendergast, P. C.; Robinson, L. L.; Bockman, M. R.; Bates, F. S.; Reineke, T. M. Bottlebrush Polymer Excipients Enhance Drug Solubility: Influence of End-Group Hydrophilicity and Thermoresponsiveness. *ACS Macro Lett.* **2021**, *10*, 375−381.
(25) Hörtz, C.; Birke, A.; Kaps, L.; Decker, S.; Wächtersbach, E.; Fischer, K.; Schuppan, D.; Barz, M.; Schmidt, M. Cylindrical Brush Polymers with Polysarcosine Side Chains: A Novel Biocompatible Carrier for Biomedical Applications. *Macromolecules* **2015**, *48* (7), 2074−2086.
(26) Wang, Y.; Wang, D.; Jia, F.; Miller, A.; Tan, X.; Chen, P.; Zhang, L.; Lu, H.; Fang, Y.; Kang, X.; Cai, J.; Ren, M.; Zhang, K. Self-Assembled DNA-PEG Bottlebrushes Enhance Antisense Activity and Pharmacokinetics of Oligonucleotides. *ACS Appl. Mater. Interfaces* **2020**, *12* (41), 45830−45837.
(27) Wang, D.; Lin, J.; Jia, F.; Tan, X.; Wang, Y.; Sun, X.; Cao, X.; Che, F.; Lu, H.; Gao, X.; Shimkonis, J. C.; Nyoni, Z.; Lu, X.; Zhang, K. Bottlebrush-Architectured Poly(Ethylene Glycol) as an Efficient Vector for RNA Interference in Vivo. *Sci. Adv.* **2019**, *5* (2), eaav9322.
(28) Lu, X.; Tran, T. H.; Jia, F.; Tan, X.; Davis, S.; Krishnan, S.; Amiji, M. M.; Zhang, K. Providing Oligonucleotides with Steric Selectivity by Brush-Polymer-Assisted Compaction. *J. Am. Chem. Soc.* **2015**, *137* (39), 12466−12469.
(29) Müllner, M.; Dodds, S. J.; Nguyen, T. H.; Senyschyn, D.; Porter, C. J. H.; Boyd, B. J.; Caruso, F. Size and Rigidity of Cylindrical Polymer Brushes Dictate Long Circulating Properties in Vivo. *ACS Nano* **2015**, *9* (2), 1294−1304.
(30) Prabha, S.; Arya, G.; Chandra, R.; Ahmed, B.; Nimesh, S. Effect of Size on Biological Properties of Nanoparticles Employed in Gene Delivery. *Artif. Cells, Nanomed., Biotechnol.* **2016**, *44* (1), 83−91.
(31) Kumar, R.; Le, N.; Tan, Z.; Brown, M. E.; Jiang, S.; Reineke, T. M. Efficient Polymer-Mediated Delivery of Gene-Editing Ribonucleoprotein Payloads through Combinatorial Design, Parallelized Experimentation, and Machine Learning. *ACS Nano* **2020**, *14* (12), 17626−17639.
(32) Sprouse, D.; Reineke, T. M. Investigating the Effects of Block versus Statistical Glycopolycations Containing Primary and Tertiary Amines for Plasmid DNA Delivery. *Biomacromolecules* **2014**, *15* (7), 2616−2628.
(33) Gori, J. L.; Hsu, P. D.; Maeder, M. L.; Shen, S.; Welstead, G. G.; Bumcrot, D. Delivery and Specificity of CRISPR/Cas9 Genome Editing Technologies for Human Gene Therapy. *Hum. Gene Ther.* **2015**, *26* (7), 443−451.
(34) Grandinetti, G.; Reineke, T. M. Exploring the Mechanism of Plasmid DNA Nuclear Internalization with Polymer-Based Vehicles. *Mol. Pharmaceutics* **2012**, *9* (8), 2256−2267.

https://doi.org/10.1021/acsmacrolett.1c00335
ACS Macro Lett. 2021, 10, 886−893